Pair Potential of Charged Colloidal Stars

F. Huang,[1] K. Addas,[2,*] A. Ward,[1] N. T. Flynn,[3] E. Velasco,[4] M. F. Hagan,[1] Z. Dogic,[1,2] and S. Fraden[1]

[1]*Department of Physics, Brandeis University, Waltham, Massachusetts 02454, USA*
[2]*Rowland Institute at Harvard, Cambridge, Massachusetts 02142, USA*
[3]*Department of Chemistry, Wellesley College, Wellesley, Massachusetts 02481, USA*
[4]*Departamento de Física Teórica de la Materia Condensada, Universidad Autónoma de Madrid, E-28049 Madrid, Spain*

(Received 22 September 2008; published 10 March 2009)

We report on the construction of colloidal stars: 1 μm polystyrene beads grafted with a dense brush of 1 μm long and 10 nm wide charged semiflexible filamentous viruses. The pair interaction potentials of colloidal stars are measured using an experimental implementation of umbrella sampling, a technique originally developed in computer simulations in order to probe rare events. The influence of ionic strength and grafting density on the interaction is measured. Good agreements are found between the measured interactions and theoretical predictions based upon the osmotic pressure of counterions.

DOI: 10.1103/PhysRevLett.102.108302 PACS numbers: 82.70.Dd

In this Letter, we describe ''colloidal stars'', which are analogous to star polymers [1–4], constructed by grafting M13 viruses [5] to polystyrene spheres. The viruses are rodlike, semiflexible charged polymers of length $L = 880$ nm, diameter $D = 6.6$ nm, and persistence length ~ 2 μm [6] with a linear charge density of $\sim 7e^-/\text{nm}$. The M13 are rigid enough to form liquid crystals [7], but when grafted to a sphere remain flexible enough to be distorted by the director field, as shown in Fig. 1. Stiffer than DNA [8], these viral brushes represent a new class of stars.

The interaction potential is probed using laser tweezers. To extract the steeply varying pair-potential we develop a new experimental protocol based on the computer simulation method known as umbrella sampling [9], but modified to increase the protocol's efficiency under experimental constraints. This new method allows the measurement of both attractive and repulsive potentials of much greater magnitude than with single line traps [10,11] and obtains comparable results to multiple holographic line traps [12]. We find that the measured potential of the colloidal stars can be modeled as arising from the osmotic pressure of the counterions, which is in several-fold excess of the repulsion due to rod excluded volume.

M13 bacteriophage was grown and purified as described elsewhere [13]. The M13 capsid protein pIII, present only on one end of the virus, was modified in order to display cysteine residues. We achieved this through making use of the Ph.D.-C7C Phage Display Peptide Library (M13-C7C, New England Biolabs, Beverly, MA) [5]. We were able to create colloidal stars with core sizes varying from 10 nm to 1 μm. Figures 1(a) and 1(b) show M13-C7C viruses conjugated with 10-nm colloidal Au particles (Ted Pella, Redding, CA). In this article, we focus on the colloidal star constructed by attaching the engineered phages to a 1 μm diameter polystyrene sphere. This was done using the following procedure: First, 230 μl of 8.8 mg/ml M13-C7C was reduced with 2 μl of 0.18 mg/ml TCEP (Tris(2-carboxyethyl) phosphine) for 15 min. This M13-C7C solution was mixed with 2 μl of 19 mM maleimide-PEO_2-biotin (Pierce, Rockford, IL) for 1 h in 20 mM phosphate buffer at pH = 7.0. The phage solution was dialyzed extensively against phosphate buffer to remove excess biotin and the pH was readjusted to 8.0. Subsequently, the phages were mixed for 1 h with 1 mg/ml Alexa Fluor® 488 carboxylic acid succinimidyl ester (Molecular Probes, Eugene, OR), and centrifuged 4 times at 170, 000g for 1 h to remove free dye molecules. 0.5 mg/ml of the fluorescently labeled viruses were then incubated with 0.5% wt vol straptavidin-coated polystyrene beads of diameter $d = 0.97 \pm 0.02$ μm (Bangs Laboratories, Fishers, IN) for 24 hours at room temperature. To the suspension 0.05 mg/ml α-casein (Sigma, St. Louis, MO) was added and the whole mixture was centrifuged twice at 20 000g for 10 min. Finally, the pellet was resuspended in 100 μl of phosphate buffer (5 mM, pH 8.0) and stored at 4 °C. The number of the sphere-bound viruses was determined using a fluorescence spectrophotometer (F-2000, Hitachi, Tokyo, Japan). By varying the stoichiometric ratio of biotinylated viruses to streptavidin-coated beads we created star polymers of different grafting densities as revealed by both fluorescence and TEM images [Figs. 1(c)–1(e)]. Fluorescence images were taken on a fluorescence microscope (TE2000-U, Nikon) equipped with a 100× oil-immersion objective and a cooled CCD camera (CoolSnap HQ, Roper Scientific). The TEM samples, stained with 2% uranyl acetate, were imaged with a 268 microscope (Morgagni, FEI Company, Hillsboro, OR), operating at 80 kV.

At the grafting density of 135 phages/bead [Fig. 1(e)], the anchored dye-labeled rods form a spherically symmetric corona around the bead with a radially averaged intensity (RAI) profile shown in Fig. 1(f). We model the phage-grafted bead as rigid, hard rods anchored to the sphere with a Gaussian angle distribution, which is centered around the surface normal. The diffraction-limited fluorescence image of the colloidal star was computed by convolving the

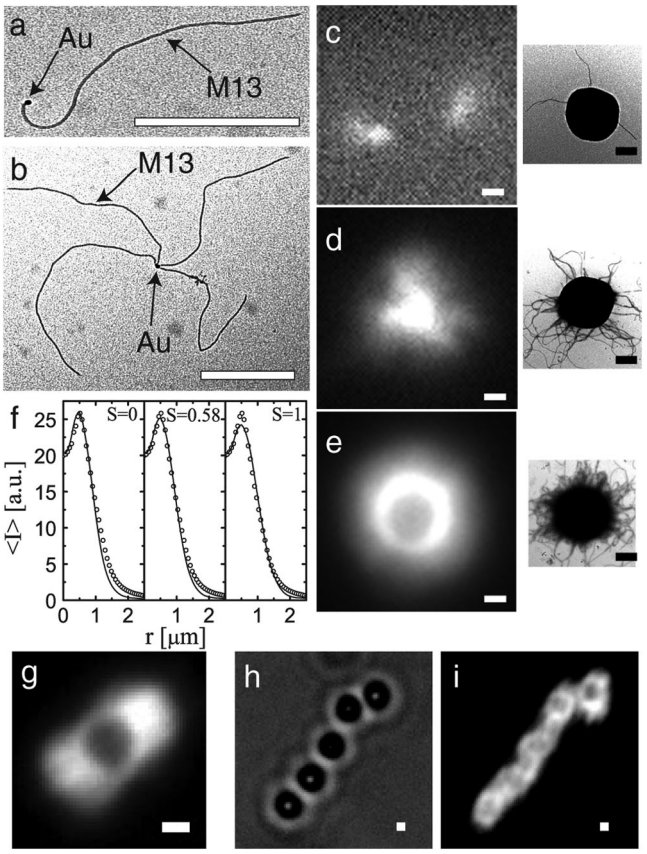

FIG. 1. (a) and (b) TEM images of 10 nm Au-bound M13 viruses of different nanoarchitectures. (c)–(e) TEM (right panel) and fluorescence (left panel) images of labeled phage grafted to unlabeled 1 μm PS beads with varying grafting densities. (c) 3 phages/bead. (d) 38 phages/bead. (e) 135 phages/bead. (f) Radially averaged fluorescent intensity profiles of the phage-grafted bead. Symbols: experiment; Solid curve: theoretical calculation with varying orientational order parameters $S = \frac{1}{2} \times \langle 3\cos^2\theta - 1 \rangle$, of anchored rods. (g) Fluorescent image of colloidal star in a M13 nematic [in contrast to (e) where the solvent is isotropic]. The "hair" grafted to the bead is "combed" parallel to the director by the nematic. (h) Brightfield image of colloidal stars associating end-to-end in a M13 nematic. (i) Fluorescent image of (h). The combed stars associate in chains aligned parallel to the nematic director with surfaces separated by a micron. Bare spheres in a nematic also assemble into chains, but with surfaces in contact. The scale bars are 500 nm.

distribution of the rod's segments with the theoretical 3D point spread function (PSF) of the microscope [14], shown in Fig. 1(f). The best fits were for intermediate order parameters.

The potential of mean force as a function of separation between two colloidal particles $W_{\text{int}}(r)$ can be determined up to an additive offset by the Boltzmann relation, $P(r) \sim \exp[-W_{\text{int}}(r)/k_BT]$. Experimentally this is accomplished by measuring the probability $P(r)$ of finding the particles at a separation r. However, for states of even moderate repulsive interaction energies $P(r)$ becomes very small, which limited the magnitude of measured potentials in previous implementations of line traps, or single bias potentials to about $6k_BT$ [10,11]. In this Letter the maximum measured potential is $40k_BT$, but we estimate that potentials several times this value are feasible with the laser power and optical resolution of our instrument.

We achieve these measurements by employing the method of umbrella sampling, in which a biasing force is used to enhance sampling of rare configurations; results are then reweighted to obtain the physical probability distribution [9]. Specifically, we place two colloidal stars [Fig. 2(b)] in separate laser traps and measure the histogram of separation distances between the colloids. The measurement is performed in a series of windows, each of which uses a different separation distance between the minima of the two laser traps. In each window the stars fluctuate about the minimum of a total potential resulting from a combination of the dual traps and interparticle star potential. Only $6k_BT$ of each of the total potentials is sampled and each minimum has a different energy, but here we show how the total potentials from overlapping windows can be combined to produce a single interparticle pair-potential of large range and magnitude. For the protocol typically used in simulations, results from different windows would be simultaneously reweighted and stitched together to obtain a continuous function for the probability $P(r)$ using the weighted histogram analysis method (WHAM) [15]. However, the biasing potential is a function of two coordinates because the position of each bead is controlled by a separate trap. The number of independent measurements required for a particular level of statistical accuracy using WHAM rises exponentially with the number of dimensions of the biasing potential. We overcome this limitation as follows.

Our goal is to measure the interaction potential, $W_{\text{int}}(r)$ with $r \equiv x_2 - x_1$, between a pair of functionalized particles sitting at positions (x_1, x_2) in a bias potential (laser traps) of strength $U_{\text{bias}}(x_1, x_2)$. We achieve this goal by performing two experiments [Fig. 2(a)]. In one experiment we place two colloidal stars in two separate laser traps and

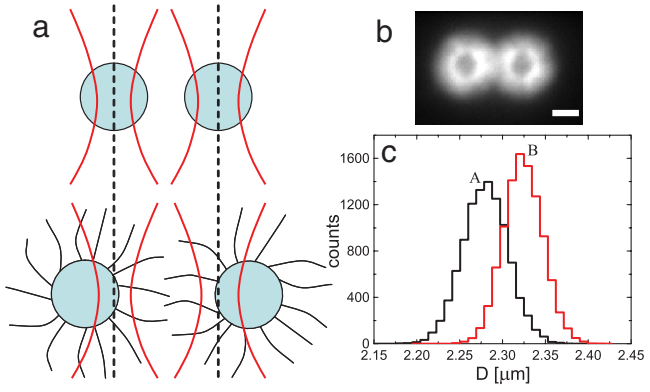

FIG. 2 (color online). Excluded volume interaction of anchored rods. (a) the schematic and (b) the fluorescence image of phage-grafted beads in optical traps. (c) separation histograms of (A) bare beads and (B) phage-grafted beads for the same trap locations. The scale bar in (b) is 1 μm.

in the other experiment we place two bare colloids in the same two traps. For both experiments we measure the separation histogram of the colloids. The potential of mean force, $W_{\rm sub}$, is then obtained by subtracting the results from each experiment.

$$W_{\rm sub}(\hat{r})/k_BT = -\log[f_f(\hat{r})] + \log[f_{\rm nf}(\hat{r})], \quad (1)$$

with $f_f(\hat{r})$ and $f_{\rm nf}(\hat{r})$ the fraction of measured displacements that fall within the histogram bin associated with the displacement value $\hat{r}$ for functionalized and nonfunctionalized beads, respectively. While this subtraction method has been used in previous experiments [10,11], we rigorously prove its validity here and show how to implement it over multiple windows.

The fractions of measured displacements are governed by the Boltzmann distribution

$$f_{\rm nf}(\hat{r}) = Z_{\rm nf}^{-1} \int dx_1 \int dx_2 e^{-U_{\rm bias}(x_1,x_2)/k_BT} \delta(x_1 - x_2 - \hat{r}) \quad (2)$$

and

$$f_f(\hat{r}) = Z_f^{-1} \int dx_1 \int dx_2 e^{-U_{\rm bias}(x_1,x_2)/k_BT} \times e^{-W_{\rm int}(x_2-x_1)/k_BT} \delta(x_1 - x_2 - \hat{r}) \quad (3)$$

with

$$Z_{\rm nf} = \int dx_1 \int dx_2 e^{-U_{\rm bias}(x_1,x_2)/k_BT}$$
$$Z_f = \int dx_1 \int dx_2 e^{-U_{\rm bias}(x_1,x_2)/k_BT} e^{-W_{\rm int}(x_2-x_1)/k_BT}. \quad (4)$$

We change the integration variables to x_1 and $r \equiv x_2 - x_1$, integrate over r, and insert the result into Eq. (1) to obtain

$$W_{\rm sub}(\hat{r}) = W_{\rm int}(\hat{r}) + k_BT \log(Z_f/Z_{\rm nf}). \quad (5)$$

We see that $W_{\rm sub}(\hat{r}) = W_{\rm int}(\hat{r})$ plus a constant. As discussed above, the strength of the laser traps, $U_{\rm bias}(x_1, x_2)$, is such that the colloids sample only a small range and therefore only a small piece of the interaction potential $W_{\rm int}(\hat{r})$ is obtained. To determine a wider range of $W_{\rm int}(\hat{r})$ the laser trap separation is varied and $W_{\rm sub}(\hat{r})$ is obtained anew. Although the constant term is different for each separation of the traps, the entire potential can be stitched together to within a single additive constant by assuming that $W_{\rm int}(\hat{r})$ is continuous. As a check of this implementation of the umbrella sampling algorithm, we used computer simulations to model the experiment. The results validating this method are shown in Fig. 3(d).

The experimental system is shown schematically in Fig. 2(a). The fluorescence image of trapped beads is shown in Fig. 2(b). Optical tweezers setup is built around an inverted fluorescence microscope. A single laser beam is time-shared between two points via a pair of orthogonally oriented paratellurite (TeO_2) acousto-optic deflectors (AOD, Intra-Action, Bellwood, IL). About 30 mW of a 1064-nm laser (Laser Quantum, Cheshire, UK) is projected onto the back focal plane of an oil-immersion objective (100 ×, N.A. = 1.3, Nikon) and subsequently focused into the sample chamber. Spheres are trapped 5 μm away from the surface to minimize possible wall effects. We choose a set of umbrella window potentials by systematically varying the locations of the traps' centers $\mathbf{r}_{c1}$ and $\mathbf{r}_{c2}$. For each window potential, six minutes of video are recorded for a pair of phage-grafted beads, and the separation probability distribution, $f_f(\hat{r})$ is obtained. It is a simple Gaussian if the separation is large and the beads are not interacting. The distances between trap positions are selected so that there are sufficient overlaps between adjacent positions. We collected data for ~30 different trap positions with 50 nm increments in separation to cover a wide range of the interparticle potential. Under identical conditions (microscope illumination, laser power, sample buffer, etc.), the experiment was repeated immediately for a pair of streptavidin-coated PS beads without attached virus to measure $f_{\rm nf}(\hat{r})$. For all experiments, statistically

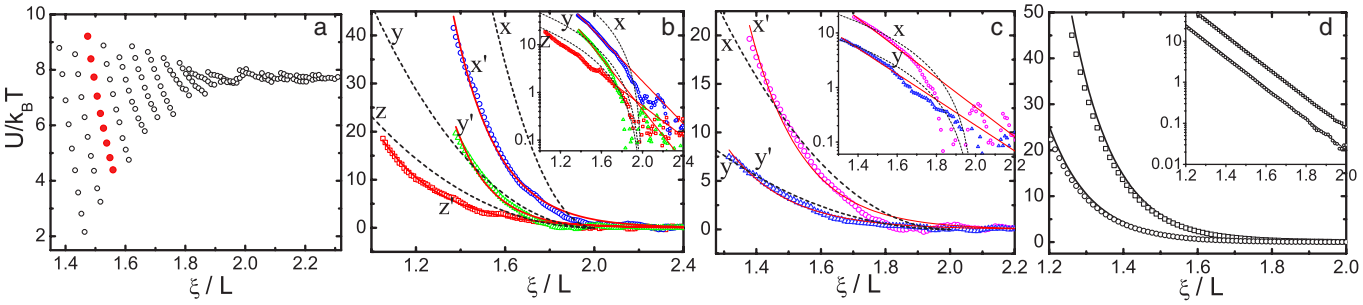

FIG. 3 (color online). (a) A set of interaction potentials of M13-grafted micron-sized polystyrene spheres acquired from each umbrella window, with the ionic strength $I = 14$ mM and the grafting density $\sigma = 135$ phages/bead. The solid symbols indicate the potential extracted from the histograms shown in Fig. 2(c). (b) Pair interaction potentials of colloidal stars at varying solution ionic strengths with $\sigma = 135$ phages/bead. Symbols: experiment; dashed lines: theory; solid lines: single exponential fits. (○, x') and (x): 2.8 mM; (△, y') and (y): 14 mM; (□, z') and (z): 28 mM. (c) Pair potentials at different grafting densities with $I = 14$ mM. (○, x') and: 135 phages/bead; (△, y') and (y): 80 phages/bead. (d) Interaction potentials $U/k_BT = Be^{-10(r-2.2)}$ employed in the Langevin dynamics simulation (solid lines) and bias potential $U_{\rm bias}(\mathbf{r}_1, \mathbf{r}_2) = \frac{1}{2}k_1|\mathbf{r}_1 - \mathbf{r}_{c1}|^2 + \frac{1}{2}k_2|\mathbf{r}_2 - \mathbf{r}_{c2}|^2$. Pair potentials extracted using the umbrella sampling (empty symbols). $B = 6$ (circle) and 20 (square). Insets: data replotted to facilitate comparison. ξ is the separation between the surfaces of spheres and L the virus length.

independent configurations of beads were sampled at 30 frames/sec. We analyzed the video images using a custom program written in the language IDL [16]. By constructing a histogram of center-center separations on 10^4 images in each window, we found clear differences between the separation probability distributions of virus-grafted beads $f_f(\hat{r})$ and bare beads $f_{\mathrm{nf}}(\hat{r})$ [Fig. 2(c)].

Figure 3(b) shows the interaction potentials measured between two M13-grafted microspheres with varying solution ionic strengths. The interactions are all purely repulsive and strongly depend on ionic strength. The potential decays to zero as the distance between sphere surfaces increases beyond twice the virus length. We compare the interaction potential between microspheres at grafting densities of 80 and 135 viruses per sphere [Fig. 3(c)]. The increase in density by 68% increases the pair potential by a factor of 2.6, but does not change its functional form.

We calculated the interaction potential arising from the osmotic pressure of counterions trapped within the grafted layers based on the mean field calculation theory of Jusufi [1–3], except modified for the case where the density of fixed charges on the grafted rods is small compared to the salt concentration. In particular, the densities of positive and negative ions within the grafted layer $\rho_{\pm}(r)$ are given by $\rho_{\pm} \approx \rho_s \pm 0.5\rho_f(r)$, with ρ_s the salt concentration and $\rho_f(r) = \lambda_f N_f/(4\pi r^2)$ the fixed concentration of negative charges on the grafted rods, with N_f the number of rods per colloid and $\lambda_f = 1.7e^-/\mathrm{nm}$ an adjustable parameter for the linear charge density renormalized by condensation. The counterion excess free energy is calculated using the Donnan equilibrium by integrating over the volume of the grafted layer $k_BT \int_0^{\pi} d\theta \sin\theta \int_{R_c}^{R_c+L_g(\theta,\xi_c)} dr r^2 \rho_f(r)^2/(2\rho_s)$ with $R_c = 0.5\mu$m the core radius, θ the angle with the center to center vector for the pair of colloids, and $\xi_c = \xi + 2R_c$ the center to center distance. Following the interaction geometry depicted in Fig. 5 of Ref. [3], the height of the grafted layer is $L_g = L$ for $\theta \geq \theta_0$ and $L_g = \xi_c/(2\cos\theta) - R_c$ for $\theta < \theta_0$ with $\cos\theta_0 = 0.5\xi_c/(L + R_c)$. We have assumed $\rho_f \ll \rho_s$ and that the height of the unperturbed grafted layer is equal to the length of a virus, $L = 880$ nm (i.e., we neglect rod orientational fluctuations). Theory and experiment are compared in Figs. 3(b) and 3(c); the agreement is rather good considering five measured potentials are fit with one value of the effective charge. However, note the discrepancy between theory and experiment at the ionic strength $I = 2.8$ mM even though the concentration of fixed charges is still small compared to the salt concentration.

We also calculated the interaction due to the excluded volume of grafted rods based on the Onsager second virial expansion of the free energy [17]. For two rods, each with a specified orientation, we find the pairwise excluded area, or the space of relative grafting locations for which the rods overlap. The calculated interaction potential due to rod excluded volume was significantly smaller than the interaction due to counterion osmotic pressure.

In conclusion, the computer simulation umbrella sampling method is implemented as an experimental protocol to extract the pair potential of colloidal stars which are trapped with optical tweezers thereby blurring the line between simulation and experiment. This method allows measurement of potentials of the order of $100k_BT$. The large measured repulsive energy between colloidal stars is consistent with the osmotic pressure of counterions between the charged brush, while a second virial theory based on the Onsager approximation significantly underestimates the pair potential. The construction of colloidal star polymers from genetically engineered viruses opens the possibility of a systematic study of hybrid colloidal materials exhibiting complex phase behaviors.

We acknowledge the help of Dr. K. Purdy and Dr. C. Xu and financial support from NSF (DMR-0444172), NSF (DMR-0705855) and NSF-MRSEC (DMR-0820492).

*Present address: Department of Physics, The American University in Cairo, P.O. Box 74 New Cairo 11835, Egypt.

[1] P. Pincus, Macromolecules **24**, 2912 (1991).
[2] A. Jusufi, C. N. Likos, and H. Löwen, J. Chem. Phys. **116**, 11 011 (2002); G. Dominguez-Espinosa *et al.*, Polymer **49**, 4802 (2008).
[3] A. Jusufi, C. N. Likos, and M. Ballauff, Colloid Polym. Sci. **282**, 910 (2004).
[4] M. Ballauff and O. Borisov, Curr. Opin. Colloid Interface Sci. **11**, 316 (2006), and references therein.
[5] C. B. Mao *et al.*, Science **303**, 213 (2004).
[6] A. S. Khalil *et al.*, Proc. Natl. Acad. Sci. U.S.A. **104**, 4892 (2007); L. Song *et al.*, Biopolymers **31**, 547 (1991).
[7] Z. Dogic and S. Fraden, Curr. Opin. Colloid Interface Sci. **11**, 47 (2006).
[8] K. Kegler, M. Salomo, and F. Kremer, Phys. Rev. Lett. **98**, 058304 (2007).
[9] G. M. Torrie and J. P. Valleau, J. Comput. Phys. **23**, 187 (1977).
[10] J. C. Crocker *et al.*, Phys. Rev. Lett. **82**, 4352 (1999).
[11] K. H. Lin *et al.*, Phys. Rev. Lett. **87**, 088301 (2001).
[12] M. Polin, Y. Roichman, and D. G. Grier, Phys. Rev. E **77**, 051401 (2008).
[13] T. Maniatis, J. Sambrook, and E. F. Fritsch, *Molecular Cloning: A Laboratory Manual* (Cold Spring Harbor Laboratory Press, Plainview, NY, 1989), 2nd ed.
[14] M. Born and E. Wolf, *Principles of Optics* (Cambridge University Press, Cambridge, England, 1997), 6th ed.
[15] A. M. Ferrenberg and R. H. Swendsen, Phys. Rev. Lett. **63**, 1195 (1989); S. Kumar *et al.*, J. Comput. Chem. **13**, 1011 (1992); B. Roux, Comput. Phys. Commun. **91**, 275 (1995).
[16] J. C. Crocker and D. G. Grier, J. Colloid Interface Sci. **179**, 298 (1996).
[17] L. Onsager, Ann. N.Y. Acad. Sci. **51**, 627 (1949).